Hyperfine structure in the $6\,^2D_{3/2}$ and $6\,^2D_{5/2}$ states of ^{87}Rb and ^{85}Rb

J. R. Brandenberger* and R. E. Lindley
Department of Physics, Lawrence University, Appleton, Wisconsin 54911, USA
(Received 24 April 2015; published 19 June 2015)

Improved measurements of hyperfine splittings in the $6\,^2D_{3/2}$ and $6\,^2D_{5/2}$ states of ^{87}Rb and ^{85}Rb have been performed using Doppler-free, double-resonance, optical pumping laser spectroscopy. The small sizes of the splittings and their associated coupling constants limit the fractional precision of the results, but when these results are combined with past measurements and scaling rules, they provide a reasonably complete and satisfactory characterization of the entire hyperfine structure in the $6\,^2D_{3/2}$ and $6\,^2D_{5/2}$ manifolds of ^{87}Rb and ^{85}Rb.

DOI: 10.1103/PhysRevA.91.062505 PACS number(s): 32.10.Fn, 32.30.−r, 32.70.−n

I. INTRODUCTION

Measurements and calculations of fine and hyperfine structures in alkali atoms have contributed significantly to our understandings of atomic structure and fundamental physics, and they have shed light on issues ranging from relativistic to configuration-mixing, electron-correlation, and core-polarization contributions to atomic structures [1–5]. While the hyperfine structures (hfs) in the $5\,^2S_{1/2}$ and $5\,^2P_J$ states of ^{87}Rb and ^{85}Rb are extremely well known [6], and recent work has improved our knowledge of the hfs in the $4\,^2D_J$ and $5\,^2D_J$ states [7,8], hyperfine structure in the higher-lying $n\,^2D_J$ states of rubidium has attracted comparatively little attention. Several measurements of hyperfine structure in the $6\,^2D_J$ states of rubidium have been reported over the years [9], but there has been little recent effort to improve and extend these measurements so as to develop a comprehensive picture of the hfs in both the $6\,^2D_{3/2}$ and $6\,^2D_{5/2}$ manifolds of ^{87}Rb and ^{85}Rb. To reverse this situation, we have employed double-resonance optical pumping (DROP) laser spectroscopy [7] to measure hyperfine splittings in the $6\,^2D_J$ states of both isotopes. When the measurements reported here are combined with past results, a reasonably complete and consistent characterization of the hyperfine structure spanning the entire $6\,^2D_J$ manifold in ^{87}Rb and ^{85}Rb emerges—a characterization that should pave the way for continued experimental and theoretical activity in the area.

II. EXPERIMENTAL ARRANGEMENT

The two-step excitation scheme and associated experimental layout used in this work are shown in Fig. 1. The target is a Rb cell 20 cm in length, maintained at 23 °C, and shielded magnetically by two layers of high-μ material. Prior to optical pumping, the number density of ^{87}Rb atoms in the $5\,^2S_{1/2}(F=2)$ ground state is about 10^9 atoms/cm^3 while that of the ^{85}Rb atoms in the $5\,^2S_{1/2}(F=3)$ ground state is three times greater. Laser 1, an external-cavity diode laser (ECDL) operating near 780.03 nm [10], is locked to the $5\,^2S_{1/2}(F=2)$ to $5\,^2P_{3/2}(F=3)$ resonance line for ^{87}Rb and the $5\,^2S_{1/2}(F=3)$ to $5\,^2P_{3/2}(F=4)$ resonance line for ^{85}Rb. Since these resonance lines are by far the strongest hfs transitions originating in the $5\,^2S_{1/2}$ states, it follows that these excitations select ^{87}Rb or ^{85}Rb atoms primarily from velocity groups with $v_{||} \approx 0$ relative to the 780.03 nm beam. Obviously these atoms, once promoted into the $5\,^2P_{3/2}$ state, continue to exhibit $v_{||} \approx 0$ velocities. In short, Laser 1 performs both velocity selection and state preparation in generating $5\,^2P_{3/2}$ atoms. Since the locking of Laser 1 involves the DAVLL method [11], the 780.03 −nm light contains no frequency modulation.

Laser 2 promotes the $5\,^2P_{3/2}$ atoms into various $6\,^2D_{3/2}$ and $6\,^2D_{5/2}$ hyperfine states by sweeping frequency near $\lambda =$ 629.923 nm and 629.835 nm, respectively. The collimated, linearly polarized, and nominally 2-mm-diameter beams from both lasers overlap and counterpropagate through the Rb cell. A second beam from Laser 2 passes through a hemispheric Fabry-Perot interferometer whose function resembles that of a plane-parallel Fabry-Perot cavity of length 16 m. This cavity consists of a 90% reflecting planoconcave mirror with radius of curvature 6.0 m located 1.5 m from a 90% reflecting plane mirror; its small free spectral range (FSR) of 16.659(5) MHz is critical since the splittings that we measure are on the order of 10 MHz. We use the uniformly spaced comb of interference fringes produced by this cavity to measure the frequency separations between the hfs spectral features that are manifest in the 780.03-nm transmission spectra.

Both lasers are custom-designed, external-cavity, Littrow-configured, diode lasers that employ commercially available diodes [12]. Their output powers are 10–30 mW before attenuation to beam intensities of several μW/cm^2; the spectral widths of these lasers are roughly 1MHz. Acquisition of the 780.03-nm spectra involves monitoring the 780.03-nm transmission through the Rb cell with a silicon PIN diode, transimpedance amplifier, and analog oscilloscope whose internal ramp sweeps Laser 2. The resulting 10-mV-high spectra, acquired via laser sweeps of 100 MHz, exhibit signal-to-noise (S/N) ratios of about 10. For S/N enhancement, these spectra are averaged by a computer-based oscilloscope with high sampling rate and 10-bit resolution. By averaging 20 sweeps, we enhance the S/N ratio to about 40. The resulting line shapes consist of 5000 points.

Figure 2 shows how the transmission of the 780.03-nm beam through a ^{87}Rb target varies with experimental conditions. In segment A both the 780.03- and 629.835-nm beams are blocked so that the absence of light falling on the PIN detector generates a quiescent baseline of zero. Then in segment B, during which the 629.835 nm beam remains blocked, the 780.03-nm beam is unblocked but detuned far off

*Corresponding author: brandenj@lawrence.edu

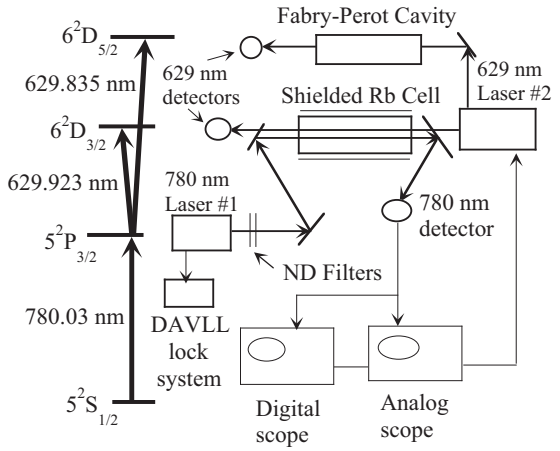

FIG. 1. Excitation scheme and physical layout for measuring hyperfine structures in the $6\,^2D_{3/2,5/2}$ states of Rb. The primary observable here is the transmission of the 780.03-nm beam passing through the Rb cell as the 629.835- or 629.923-nm counterpropagating beam scans through higher-lying resonances.

the $5\,^2S_{1/2}(F=2)$ to $5\,^2P_{3/2}(F=3)$ transition so that we detect a large amount of 780.03-nm transmission through the cell. Then in segment C, the 629.835-nm beam remains blocked but the 780.03-nm beam is locked to the $5\,^2S_{1/2}(F=2)$ to $5\,^2P_{3/2}(F=3)$ transition in ^{87}Rb. Given that the 780.03-nm transmission drops by 50% and the absorption cross section for the $5\,^2S_{1/2}(F=2)$ to $5\,^2P_{3/2}(F=3)$ transition is $\sigma = 1.356\times10^{-9}\,\mathrm{cm}^2$ [13], we infer that the number density of ^{87}Rb atoms in the $5\,^2S_{1/2}(F=2)$ state with $v_{||}\approx 0$ is roughly $2\times10^7\,\mathrm{atoms/cm}^3$. Since this transition is cycling, there is negligible optical pumping into the $5\,^2S_{1/2}(F=1)$ ground state at this point. Given that the intensity of the 780.03-nm beam, once attenuated, roughly equals the saturation intensity $I_{\mathrm{sat}} = 1.67\,\mathrm{mW/cm}^2$ [13], and since this intensity prompts upward excitation rates comparable to the $5\,^2P_{3/2}$ spontaneous decay rate $\Gamma_{21}/2\pi = 6.06\,\mathrm{MHz}$, a typical $v_{||}\approx 0$ ^{87}Rb atom involved in this excitation and relaxation process undergoes the $5\,^2S_{1/2}(F=2)$ to $5\,^2P_{3/2}(F=3)$ to $5\,^2S_{1/2}(F=2)$ cycle in roughly 50 ns (two $5\,^2P_{3/2}$ lifetimes).

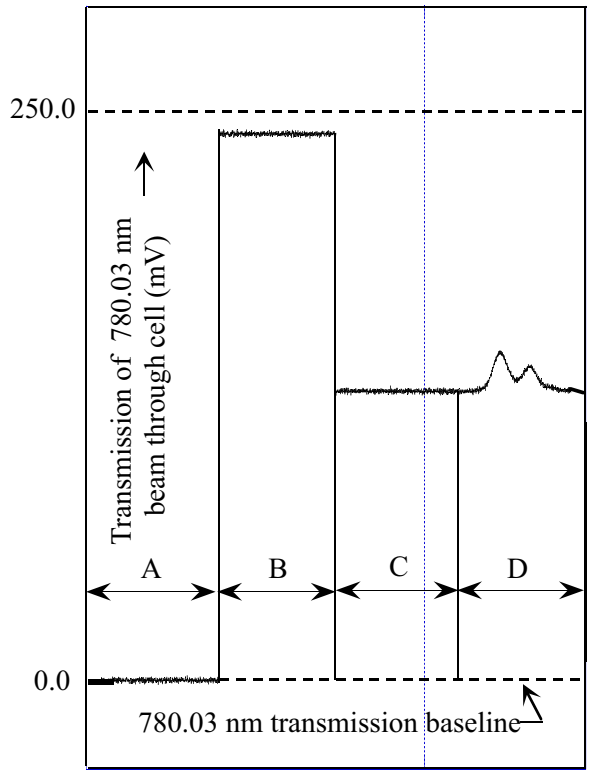

FIG. 2. (Color online) Four temporal segments A through D showing the 780.03-nm transmission under different conditions, ultimately exhibiting resonances due to the $5\,^2P_{3/2}(F=3)$ to $6\,^2D_{5/2}(F=4,3,2)$ transitions driven by the 629.835-nm beam from Laser 2.

Finally, in segment D, where the 629.835-nm beam is unblocked and scans through the $5\,^2P_{3/2}(F=3)$ to $6\,^2D_{5/2}(F=4,3,2)$ resonances, the excitation/ decay time lengthens to about 300 ns (the $6\,^2D_{5/2}$ lifetime) and thereby reduces the availability of $5\,^2S_{1/2}(F=2)$ absorbers with $v_{||}\approx 0$ as a result of the resonances and atomic shelving. But even more importantly given the DROP scheme, the existence of various return paths to the $5\,^2S_{1/2}$ ground states assures that optical pumping into the $5\,^2S_{1/2}(F=1)$ rather than $5\,^2S_{1/2}(F=2)$ ground state prompts even more 780.03-nm transmission through the cell during the resonances. This greater transmission shows up as the upward pointing transmission peaks in Fig. 2. The fractional strengths of the peaks in such spectra are 10× larger than the corresponding peaks that we observe when monitoring the 629.835-nm transmission directly. We note that the DROP method is particularly effective in alkali atoms where the pair of hyperfine-split ground states facilitates optical pumping.

III. THEORY

Hyperfine structure stems from the interaction of nuclear moments with fields produced by atomic electrons [1,14]. Viewing $\boldsymbol{J}$ and $\boldsymbol{I}$ as good quantum numbers, the magnetic dipole Hamiltonian is $H = -\boldsymbol{\mu}\cdot\boldsymbol{B}_{el}$, where $\boldsymbol{\mu}$ is the nuclear magnetic moment and $\boldsymbol{B}_{el}$ the magnetic field at the nucleus due to the electrons. Since $\boldsymbol{\mu}$ is proportional to $\boldsymbol{I}$ and $\boldsymbol{B}_{el}$ to $\boldsymbol{J}$, the Hamiltonian becomes $H = A_J\boldsymbol{I}\cdot\boldsymbol{J}$. Then to first order, the shift of a level J due to this interaction is $\Delta E = {}^1\!/_2 A_J[F(F+1) - J(J+1) - I(I+1)]$, where F is the total angular momentum. The coupling constant A_J appears in the interval rule $\Delta E(F) - \Delta E(F-1) = A_J F$, where a positive A_J indicates normal hfs ordering.

The Hamiltonian for the electric quadrupole interaction is

$$H_Q = eQ\langle\partial^2 V_e/\partial z^2\rangle[3(\boldsymbol{I}\cdot\boldsymbol{J})^2 + 3(\boldsymbol{I}\cdot\boldsymbol{J})/2 - I(I+1)J(J+1)]/[2I(2I-1)J(2J-1)], \quad (1)$$

where Q is the nuclear quadrupole moment and $\langle\partial^2 V_e/\partial z^2\rangle$ the electric-field gradient at the nucleus. This quadrupole interaction shifts the energies by

$$\Delta E = B_J[3K(K+1)/2 - 2I(I+1)J(J+1)]/4I(2I-1) \times J(2J-1), \quad (2)$$

where $K \equiv F(F+1) - J(J+1) - I(I+1)$ and B_J is the electric quadrupole coupling constant. Combining these two

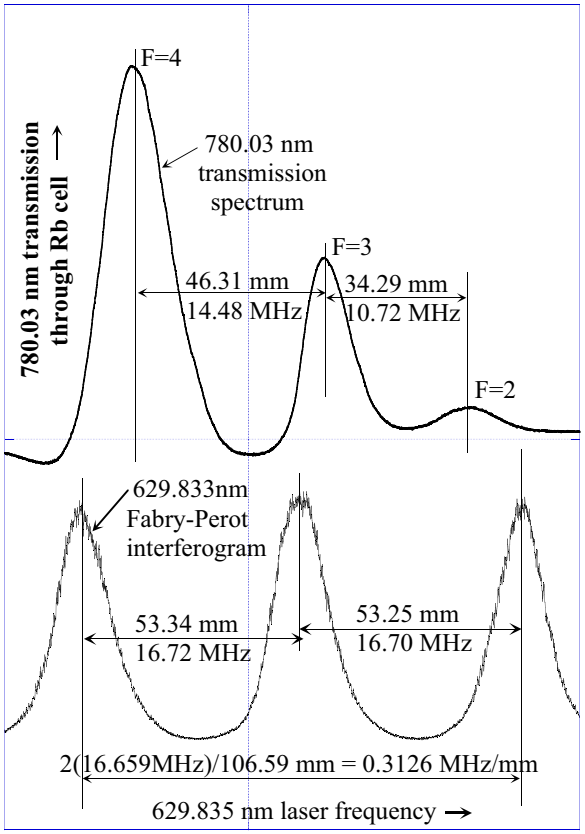

FIG. 3. (Color online) Transmission spectrum of 780.03-nm for excitation into the $6\,^2D_{5/2}(F = 4,3,2)$ states of ^{87}Rb along with an accompanying Fabry-Perot interferogram. Since two free spectral ranges (2×16.659 MHz) span 106.59 mm on the original chart, the calibration here is 0.312 MHz/mm, and the two hfs splittings in this chart are found to be $^{87}\Delta_{4,3} = 14.48$ MHz and $^{87}\Delta_{3,2} = 10.72$ MHz.

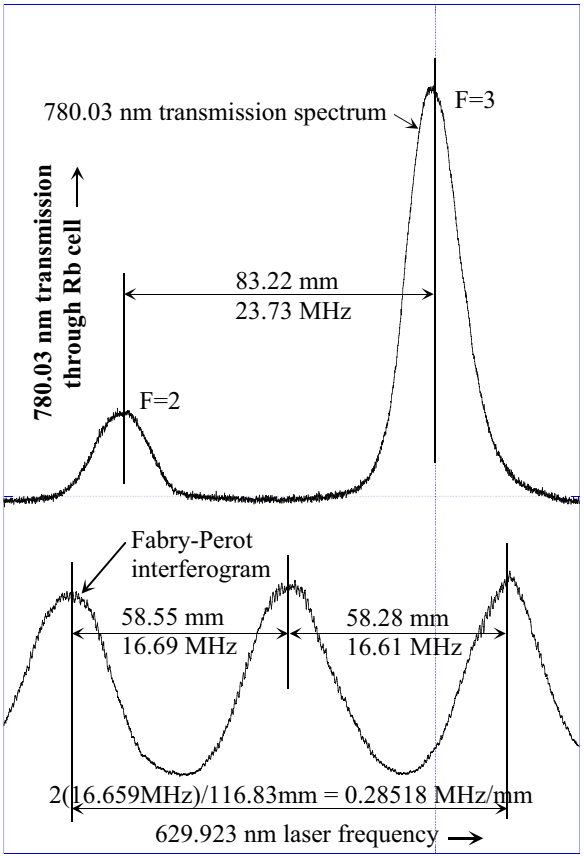

FIG. 4. (Color online) Transmission spectrum of 780.03-nm for excitation into the $6\,^2D_{3/2}(F = 2,3)$ states of ^{87}Rb along with an accompanying Fabry-Perot interferogram. Since two free spectral ranges (2×16.659 MHz) span 116.83 mm on the chart, the calibration is 0.28519 MHz/mm implying a splitting of $\Delta_{3,2} = 23.73$ MHz.

interactions, one finds that the frequency of each hyperfine sublevel F is

$$\nu_F = \nu_o + A_J K/2 + B_J[3K(K+1) - 4I(I+1) \times J(J+1)]/[8I(2I-1)J(2J-1)], \quad (3)$$

where ν_o is the frequency of the unperturbed fine-structure level. By subtracting Eq. (3) from itself for two different values of F, one derives expressions for the splittings between pairs of hyperfine levels in terms of A_J and B_J [15]. Two such expressions are then used to determine A_J and B_J.

IV. HYPERFINE SPECTRA

Examples of our 780.03-nm transmission spectra containing hyperfine features and splittings in the $6\,^2D_{3/2,5/2}$ manifolds of ^{87}Rb appear in Figs. 3 and 4. These Doppler-free spectra exhibit peaks in the transmission of the 780.03-nm beam passing through the cell—peaks that occur when Laser 2 scans through the $5\,^2P_{3/2}$ to $6\,^2D_{3/2,5/2}$ resonances. In Fig. 3, where the excitation sequence is $5\,^2S_{1/2}(F = 2)$ to $5\,^2P_{3/2}(F = 3)$ to $6\,^2D_{5/2}(F = 4,3,2)$, one finds an hfs feature for each of the three $6\,^2D_{5/2}(F = 4,3,2)$ destination states. These three features permit measurement of two hfs splittings and hence the inferring of both coupling constants A_J and B_J from a given ^{87}Rb spectrum. We have processed 75 such transmission spectra; the resulting average values for the two largest $6\,^2D_{5/2}$ hfs splittings are $^{87}\Delta_{4,3} = 14.59(18)$ MHz and $^{87}\Delta_{3,2} = 10.73(16)$ MHz, where the uncertainties are approximately equal parts statistical and systematic and represent two standard errors (95% confidence level).

In Fig. 4, where the 780.03-nm transmission spectrum stems from $5\,^2S_{1/2}(F = 2)$ to $5\,^2P_{3/2}(F = 3)$ to $6\,^2D_{3/2}(F = 2,3)$ excitation in ^{87}Rb, selection rules limit our access to just the $6\,^2D_{3/2}(F = 2)$ and $6\,^2D_{3/2}(F = 3)$ states. Hence we can extract only one hfs splitting, which in the spectrum in Fig. 4, is 23.73 MHz. We have acquired 24 such spectra; the resulting average value of the $6\,^2D_{3/2}(F = 2,3)$ splitting is $^{87}\Delta_{3,2} = 24.08(35)$ MHz, where the uncertainty is approximately equal parts statistical and systematic and represents two standard errors (95% confidence level).

Figures 5 and 6 contain 780.03-nm transmission spectra for cases involving the isotope ^{85}Rb. To acquire these spectra, Laser 1 is locked to the $5\,^2S_{1/2}(F = 3)$ to $5\,^2P_{3/2}(F = 4)$ transition in ^{85}Rb. Since the hfs splittings in the $5\,^2P_{3/2}$ manifold of ^{85}Rb are roughly half that of the corresponding splittings in ^{87}Rb, the exclusivity with which we promote mainly $v_{||} \approx 0$ atoms from the $5\,^2S_{1/2}(F = 3)$ ground state into the $5\,^2P_{3/2}(F = 4)$ state is less pronounced than in the case of

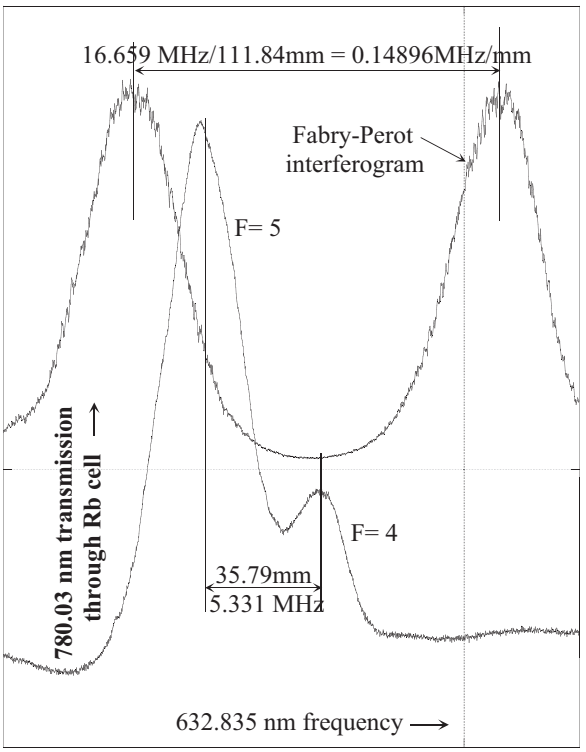

FIG. 5. Transmission spectrum of 780.03 nm for excitation into the $6\,^2D_{5/2}(F = 5,4)$ states of ^{85}Rb along with an accompanying Fabry-Perot interferogram. Since one free spectral range (16.659 MHz) spans 111.84 mm on the chart, the calibration here is 0.14896 MHz/mm implying an hfs splitting of $^{85}\Delta_{5,4} = 5.331$ MHz.

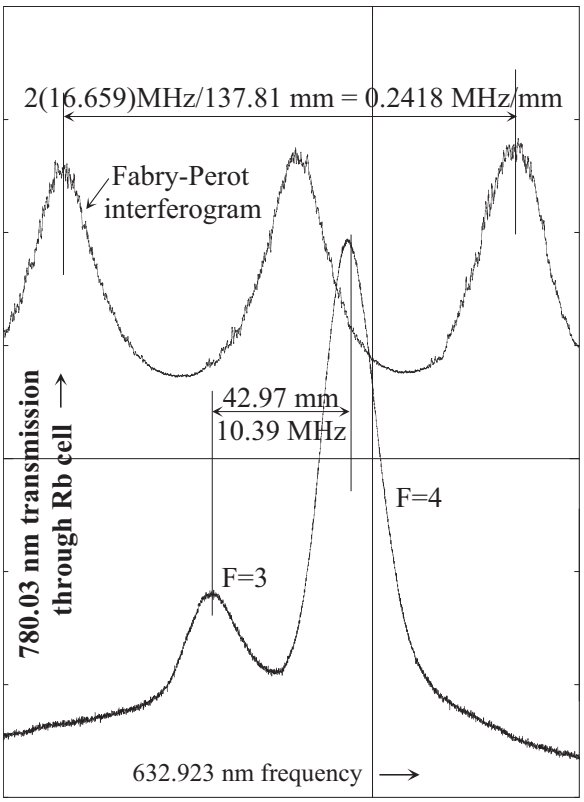

FIG. 6. Transmission spectrum of 780.03 nm for excitation into the $6\,^2D_{3/2}(F = 3,4)$ states of ^{85}Rb along with an accompanying Fabry-Perot interferogram. Since two free spectral ranges ($2 \times$ 16.659 MHz) span 137.81 mm on the chart, the calibration here is 0.2418 MHz/mm implying an hfs splitting of $^{85}\Delta_{4,3} = 10.39$ MHz.

^{87}Rb—i.e., we inevitably promote some $v \neq 0$ $5\,^2S_{1/2}(F = 3)$ atoms into the $5\,^2P_{3/2}(F = 3)$ state via Doppler shifting of the 780.03-nm incoming light. This complication, however, has negligible effect on our results.

Regarding the widths of the transmission peaks in Figs. 3–6, most are about 6 MHz FWHM. This fact suggests that our excitation process is dominated by two-step as opposed to two-photon transitions. Assuming negligible Doppler, power, transit, and collisional and laser width broadening, one expects these two-step linewidths to be dictated by the $5\,^2P_{3/2}$ and $6\,^2D_{3/2,5/2}$ lifetimes of $\tau_1 = 26.23$ ns [13] and $\tau_2 \approx 300$ ns [16]. Hence one expects a minimum two-step FWHM $= (1/\tau_1 + 1/\tau_2)/2\pi = 6.6$ MHz, which is close to what we observe.

V. RESULTS

Using average values of the hfs splittings derived from numerous spectra such as those shown in Figs. 3–6, and combining these splittings with past results, Table I presents eight hfs splittings and associated coupling constants A_J and B_J for both $6\,^2D_J$ manifolds in ^{87}Rb and ^{85}Rb. The splittings and coupling constants (all expressed in MHz) generated by the present work (either directly or indirectly via scaling) are **emboldened** in the table. The nonemboldened entries summarize the work of others.

The experimental uncertainties associated with the emboldened items in the table are approximately equal parts statistical and systematic and represent two standard errors (95% confidence level). Most of these overall uncertainties fall in the 1% range except for those related to the B_J where the larger fractional uncertainties are due mainly to the smallness of B_J. We view these uncertainties of roughly 1% as reasonable for the following reason: We claim to locate the centers of our various 6 MHz-wide features to about 2% of the widths or to 0.1 MHz (at least statistically). Then since the separations between relevant pairs of features are about 10 MHz, the resulting fractional uncertainties in the inferred splittings are about 1%.

Consider next several possible systematic contributions to these uncertainties. Figures 3–6 show that our spectral and interference peaks occasionally show modest amounts of asymmetry which we attribute to the marginal performance of Laser 2—its fast noise, mode instability, and/or occasional inclusion of secondary modes—all of which are exacerbated by scanning this laser. While Laser 1, based on an anti-reflection coated 780-nm diode, exhibits continuous, single-mode tuning of 5 GHz or more, Laser 2 demonstrates an inferior performance despite the fact that we have tried more than a dozen diodes of three different types supplied by three different manufacturers [17].

As to possible systematic errors associated with our use of the Fabry-Perot cavity with FSR = 16.659(5) MHz, we claim that any systematic error associated with its use is insignificant

TABLE I. Hyperfine splittings $\Delta_{F,F-1}$ between hyperfine levels F and F-1 in the $6\,^2D_{5/2}$ and $6\,^2D_{3/2}$ manifolds of ^{87}Rb($I = 3/2$) and ^{85}Rb($I = 5/2$) along with inferred coupling constants A_J and B_J (all measured in MHz). The results of the present work (including entries based upon scaling) are **emboldened**; their associated uncertainties are two standard errors (95% confidence level). The nonemboldened entries represent the work of others.

Isotope	State	Splitting (MHz)	Splitting (MHz)	A_J (MHz)	B_J (MHz)
^{87}Rb	$6\,^2D_{5/2}$	$\mathbf{^{87}\Delta_{4,3} = 14.59(18)}$[a]	$\mathbf{^{87}\Delta_{3,2} = 10.73(16)}$[a]	$\mathbf{^{87}A_{5/2} = -3.61(6)}$[a]	$\mathbf{^{87}B_{5/2} = -0.20(20)}$[a]
^{87}Rb	$6\,^2D_{3/2}$	$\mathbf{^{87}\Delta_{3,2} = 24.08(35)}$[b]	$^{87}\Delta_{2,1} = 15.15(12)$[b]	$^{87}A_{3/2} = 7.84(5)$[b,c]	$^{87}B_{3/2} = 0.53(6)$[b]
^{85}Rb	$6\,^2D_{5/2}$	$\mathbf{^{85}\Delta_{5,4} = 5.49(22)}$[d]	$\mathbf{^{85}\Delta_{4,3} = 4.25(7)}$[d]	$\mathbf{^{85}A_{5/2} = -1.069(18)}$[d]	$\mathbf{^{85}B_{5/2} = -0.41(41)}$[d]
^{85}Rb	$6\,^2D_{3/2}$	$\mathbf{^{85}\Delta_{4,3} = 10.36(32)}$[e]	$^{85}\Delta_{3,2} = 6.23(19)$[e]	$^{85}A_{3/2} = 2.32(6)$[c,e]	$^{85}B_{3/2} = 1.62(6)$[f]

[a]These splittings of $^{87}\Delta_{4,3} = 14.59(18)$ and $^{87}\Delta_{3,2} = 10.73(16)$ and their associated coupling constants $^{87}A_{5/2} = -3.61(6)$ and $^{87}B_{5/2} = -0.20(20)$ represent a major part of the present work. Our uncertainty of 0.06 in our $^{87}A_{5/2} = -3.61(6)$ is nearly an order of magnitude smaller than the uncertainty of Svanberg and Hogervorst in their $^{87}A_{5/2} = -3.4(5)$ [9]. Svanberg and Hogervorst quote neither hfs splittings nor a value for $^{87}B_{5/2}$.

[b]In our work, we found this value of $^{87}\Delta_{3,2} = 24.08(35)$. If one starts from Svanberg's $^{87}A_{3/2} = 7.84(5)$ and $^{87}B_{3/2} = 0.53(6)$ [9] and works backward to evaluate $^{87}\Delta_{3,2}$, the result is 24.05(16), in excellent agreement with our 24.08(35). The same backward process yields the value of $^{87}\Delta_{2,1} = 15.15(12)$. Selection rules preclude our measurement of this splitting.

[c]Svanberg's and van Wijngaarden's $^{87}A_{3/2} = 7.84(5)$ and $^{85}A_{3/2} = 2.32(6)$ [9] yield the ratio $^{87}A_{3/2}/^{85}A_{3/2} = 3.379$, in excellent agreement with Moon's value $^{87}A_{3/2}/^{85}A_{3/2} = 3.3771170962(67)$ [7].

[d]Our measured value of $^{85}\Delta_{5,4} = 5.49(22)$ agrees well with the calculated splitting $^{85}\Delta_{5,4} = 5.59(26)$, which one obtains by working backward from $^{85}A_{5/2} = -1.069(18)$ and $^{85}B_{5/2} = -0.41(41)$. The latter were obtained using Moon's scaling factors [7] and our $^{87}A_{5/2} = -3.61(6)$ and $^{87}B_{5/2} = -0.20(20)$ in the first line of the table. We quote the scaled value $^{85}A_{5/2} = -1.069(18)$ in preference to Hogervorst's less precise $^{85}A_{5/2} = -0.095(20)$ [20]. The splitting $^{85}\Delta_{4,3} = 4.25(7)$ is also a calculated value stemming from $^{85}A_{5/2} = -1.069(18)$ and $^{85}B_{5/2} = -0.41(41)$. We are unable to measure this splitting.

[e]This measured splitting $^{85}\Delta_{4,3} = 10.36(32)$ from the present work agrees well with the reverse-calculated value of 10.58(24), which can be derived from van Wijngaarden's $^{85}A_{3/2} = 2.32(6)$ and $^{85}B_{3/2} = 1.62(6)$ [21]. The adjoining splitting $^{85}\Delta_{3,2} = 6.23(19)$ is also reverse calculated starting from van Wijngaarden's $^{85}A_{3/2} = 2.32(6)$ and $^{85}B_{3/2} = 1.62(6)$ [21]. We are not able to measure this splitting directly.

[f]When this $^{85}B_{3/2} = 1.62(6)$ by van Wijngaarden [21] is combined with Svanberg's $^{87}B_{3/2} = 0.53(6)$ [9] to evaluate the ratio $^{87}B_{3/2}/^{85}B_{3/2}$, the result is 0.33(5), which disagrees with Moon's value of $^{87}B_{3/2}/^{85}B_{3/2} = 0.4838(35)$ based on recent hfs work in the $4\,^2D_{3/2,5/2}$ states of ^{87}Rb and ^{85}Rb. It appears that Svanberg's $^{87}B_{3/2} = 0.53(6)$ [9] may be small.

(much less than 1%) once we average over a large number of similar spectra. The basis for this claim is that the modest asymmetries in both our fringes and spectral features vary randomly from one spectrum and interferogram to the next. Hence we believe that the effects of these asymmetries in the fringes and peaks average out and thus become significantly less than 1% when we average a large number of similarly acquired spectra [18].

Consider a final systematic effect that does appear in the uncertainties in Table I. This effect stems from a possible nonlinearity in the scan of Laser 2, a scan that arises from the application of a highly linear sawtooth voltage ramp to the laser's piezo element. In an ideal, noise-free, linear case, the resulting separations between adjacent Fabry-Perot peaks (e.g., the 16.72-MHz and 16.70-MHz separations in Fig. 3) would be equal, a condition that we assume (at least statistically) in exploiting our Fabry-Perot interferograms to calibrate the scan and infer the splittings in our 780.03-nm spectra. To explore this matter, we have analyzed 75 interferograms similar to the lower trace in Fig. 3 so as to evaluate the *fractional change* in the separations between adjacent pairs of Fabry-Perot peaks. In the case of Fig. 3, this fractional change is $(53.34\,\text{mm} - 53.25\,\text{mm})/53.34\,\text{mm} = 0.00169$, thereby implying a possible scan nonlinearity of 0.17%.

We then average all 75 values of these fractional changes (roughly half being positive and half negative) for this set of spectra, arriving at a *mean* fractional change in separations of -0.001996, which corresponds statistically to a possible -0.1996% local nonlinearity in the sweep. Since the attendant standard error associated with this -0.001996 mean fractional change is 0.00413, one concludes that statistically for this set of 75 spectra, there is no definite demonstrable nonlinearity in the scan. When viewed at the 95% confidence level, we find that any percentage nonlinearity in this sweep of Laser 2 falls between $-0.1996\% + 2(0.413)\% = 0.627\%$ and $-0.1996\% - 2(0.413)\% = -1.026\%$. We round these results to 1% to arrive at a single systematic uncertainty associated with a possible nonlinearity in the sweep of Laser 2. Hence with respect to the inferred hfs splittings in our 780.03-nm absorption spectra, this possible level of nonlinearity affects our inferred splittings by no more than 1%. Combining this 1% systematic uncertainty in quadrature with our nominal statistical line-shape uncertainty of 1% leaves us with a composite overall uncertainty of 1.5% in our inferred frequency splittings for the ^{87}Rb $6\,^2D_{5/2}$ case and presumably a similar amount for the other results.

We add here that our use of scaling in Table I ignores the presence of hyperfine anomalies,

$$^{87}\Delta^{85} = (^{87}A_J/^{85}A_J)/(^{87}g_I/^{85}g_I) - 1, \tag{4}$$

in the $6\,^2D_J$ states. This ignoring of such anomalies is prompted by the smallness of the recently determined anomalies $^{87}\Delta^{85} \approx 0.005$ in the nearby $5\,^2D_J$ states. Anomalies of this magnitude in the present work would produce effects that would be substantially less than our nominal uncertainties of 1% [19].

VI. DISCUSSION

In assessing the results collected in Table I, we point out that there is substantial completeness and consistency among the various entries. We also note that two of the values of A_J are negative, thereby implying that the hyperfine structures in the $6\,^2D_{5/2}$ state of ^{87}Rb and $6\,^2D_{5/2}$ state of ^{85}Rb are inverted. Inverted hyperfine structures are fairly common in heavier alkali atoms where relativistic and electron-correlation contributions to hyperfine structures are often significant. A second point to notice in Table I is that the values of A_J vary considerably from one to another, which suggests that the effective magnetic fields $\boldsymbol{B}_{el}$ at the two nuclei vary substantially among the four $6\,^2D_J$ states examined here.

The electric quadrupole coupling constants B_J in Table I also vary considerably indicating that the electric-field gradients at the two nuclei vary significantly among the $6\,^2D_J$ states. For the $6\,^2D_{5/2}$ states in both ^{87}Rb and ^{85}Rb, B_J is negative indicating that the electric-field gradient has changed direction compared to the other two cases. We conclude that any further inferences drawn from the values of these splittings and couplings must await a theoretical analysis that involves treatments of relativistic, configuration-mixing, electron-correlation, and core-polarization effects.

ACKNOWLEDGMENTS

We are pleased to acknowledge discussions with Steven A. Blundell and support from the Skran Research Fund and Lawrence University.

[1] I. Lindgren and R. Rosen, Case Stud. At. Phys. **4**, 93 (1974); E. Arimondo, M. Ingusio, and P. Violino, Rev. Mod. Phys. **49**, 31 (1977); I. Lindgren and A.-M. Mårtensson, Phys. Rev. A **26**, 3249 (1982); J.-L. Heully and A.-M. Mårtensson-Pendrill, *ibid.* **27**, 3332 (1983).

[2] E. Luc-Koenig, Phys. Rev. A **13**, 2114 (1976); J. Phys (Paris) **41**, 1273 (1980).

[3] T. Lee, J. E. Rodgers, T. P. Das, and R. M. Sternheimer, Phys. Rev. A **14**, 51 (1976); R. M. Sternheimer, J. E. Rodgers, T. Lee, and T. P. Das, *ibid.* **14**, 1595 (1976).

[4] N. C. Pyper and P. Maretos, J. Phys. B **14**, 4469 (1981); D. A. Smith and I. G. Hughes, Am. J. Phys. **72**, 631 (2004); J. Wang, H. Liu, G. Yang, B. Yang, and J. Wang, Phys. Rev. A **90**, 052505 (2014); M. Krainska-Miszczak, Phys. Lett. A **160**, 85 (1991); Acta Phys. Pol., A **86**, 343 (1994).

[5] S. A. Blundell, Phys. Rev. A **90**, 042514 (2014); J. R. Brandenberger and G. S. Malyshev, *ibid.* **81**, 032515 (2010); J. R. Brandenberger, C. A. Regal, R. O. Jung, and M. C. Yakes, *ibid.* **65**, 042510 (2002).

[6] S. Bize, Y. Sortais, M. S. Santos, C. Mandache, A. Clairon, and C. Salomon, Europhys. Lett. **45**, 558 (1999).

[7] H. S. Moon, W. K. Lee, L. Lee, and J. B. Kim, Appl. Phys. Lett. **85**, 3965 (2004); H. S. Moon, L. Lee, and J. B. Kim, J. Opt. Soc. Am. B **24**, 2157 (2007); W. Lee, H. S. Moon, and H. S. Suh, Opt. Lett. **32**, 2810 (2007); H. S. Moon, W. K. Lee, and H. S. Suh, Phys. Rev. A **79**, 062503 (2009); P. Thoumany, T. Hänsch, G. Stania, L. Urbonas, and Th. Becker, Opt. Lett. **34**, 1621 (2009).

[8] F. Nez and E. Biraben, Opt. Commun. **102**, 432 (1993); F. Nez, F. Biraben, R. Felder, and Y. Millerioux, *ibid.* **110**, 731 (1994); W. Suptitz, B. C. Duncan, and P. L. Gould, J. Opt. Soc. Am. B **14**, 1001 (1997).

[9] S. Svanberg, P. Tsekeris, and W. Happer, Phys. Rev. Lett. **30**, 817 (1973); S. Svanberg and P. Tsekeris, Phys. Rev. A **11**, 1125 (1975); S. Svanberg, Hyperfine Interact. **15/16**, 111 (1983); W. A. van Wijngaarden, K. D. Bonin, and W. Happer, Phys. Rev. A **33**, 77 (1986); W. A. van Wijngaarden, J. Li, and J. Koh, *ibid.* **48**, 829 (1993).

[10] All wavelengths quoted in this paper are measured in air.

[11] K. L. Corwin, Z. T. Lu, C. F. Hand, R. J. Epstein, and C. E. Wieman, Appl. Opt. **37**, 3295 (1998).

[12] The laser diodes used in this work were supplied by Eagleyard, Ushio, Oclaro, and Qphotonics.

[13] D. A. Steck, *Rubidium Line Data*, available online at http://steck.us/alkalidata, version 2.1.4 (2010) and version 2.1.6 (2013).

[14] Lloyd Armstrong, Jr., *Theory of the Hyperfine Structure of Free Atoms* (Wiley-Interscience, New York, 1971).

[15] In the case of ^{87}Rb, Eq. (3) yields the following pair of expressions for the larger hfs splittings in the $6\,^2D_{5/2}(F = 4,3,2)$ manifold: $\Delta_{4,3} = -4\,^{87}A_{5/2} - (4/5)\,^{87}B_{5/2}$ and $\Delta_{3,2} = -3\,^{87}A_{5/2} + (9/20)\,^{87}B_{5/2}$.

[16] D. C. Morton, Astrophys. J., Suppl. Ser. **130**, 403 (2000).

[17] These shortcomings with the 629-nm laser were minimized but not eliminated because we could find no diodes worldwide that could be pulled or temperature tuned to 629.835 or 629.923 nm where they would operate single mode while scanning. Diodes that do exist in this wavelength range tend to be multimode devices unsuitable for ECLD operation. We found the available 633–638-nm diodes to be inferior to some 20 different diodes that we have previously used in ECDLs at many wavelengths. These difficulties with this 629-nm laser constitute the main reason why we view the current work as somewhat exploratory.

[18] As suggested by the vertical lines in Figs. 3–6, we determined the centers of the majority of our fringes and peaks by making careful albeit visual judgments of their centers of gravity. To test the reliability of this method, we performed least-squares fits to a representative sampling of the spectra and fringes. This test revealed that statistically the splittings stemming from visual versus least-squares fitted determinations of the centers of the peaks agreeing to within 0.3%, well below the nominal 1% uncertainties that we attach to the results in Table I.

[19] M. G. H. Gustavsson and A.-M. Martensson-Pendril, Phys. Rev. A **58**, 3611 (1998).

[20] W. Hogervorst and S. Svanberg, Phys. Scr. **12**, 67 (1975).

[21] W. A. van Wijngaarden and J. Sagle, Phys. Rev. A **45**, 1502 (1992).